BUTTERWORTH HEINEMANN

Composites **26** (1995) 403–414

0010-4361/95/$10.00

Effect of matrix cracking and interface sliding on the thermal expansion of fibre-reinforced composites

T.J. Lu and J.W. Hutchinson*
Division of Applied Sciences, Harvard University, Cambridge, MA 02138, USA
(Received 21 March 1994; revised 5 September 1994)

The effect of matrix cracking on the thermal expansion behaviour of brittle, unidirectional fibre-reinforced composites is studied. Sliding along the fibre–matrix interface accompanying matrix cracking has a major effect on the change in thermal expansion. This problem is also addressed, both with and without friction. For the most common composite systems, whose fibres have a smaller coefficient of thermal expansion than that of the matrix, matrix cracking and interface sliding result in a reduction of the thermal expansion of the composite. A cylindrical cell model of a composite with uniformly spaced matrix cracks is invoked for analysis. Shear-lag approximations, enhanced by selected finite element solutions to the cell model, provide estimates of the functional dependence of thermal expansion on constituent properties, matrix crack density and extent of sliding. Hysteresis behaviour during thermal cycling is analysed accounting for reverse frictional sliding along debonded portions of the fibre–matrix interface. A non-dimensional parameter, $E_m\Delta\alpha\Delta T/\tau$ (where E_m is the matrix modulus, $\Delta\alpha$ the thermal expansion mismatch between fibre and matrix, ΔT the amplitude of the temperature cycle and τ the frictional resistance to sliding), is identified which governs the extent to which sliding reduces the effective expansion coefficient of the composite.

(Keywords: thermal expansion coefficients; matrix cracking; interface sliding; thermal cycling; hysteresis)

INTRODUCTION

Among the first applications under consideration for ceramic matrix composites are components for jet engines which will be subject to high temperatures and temperature gradients but low mechanical loads. The thermal expansion properties of the composites will play an important role in determining the thermal stresses that these components will experience. Fibre-reinforced ceramic matrix composites are being developed to withstand stress levels in excess of the stresses at which matrix cracks form. It is expected that the components in question will experience at least limited amounts of matrix cracking in regions of high stress concentration. Since matrix cracking changes the effective thermal expansion coefficients of the composite, thermal stresses induced in the component by the high temperature environment will be affected by matrix cracking. In other words, a non-linear coupling exists wherein thermally induced stresses causing matrix cracking will themselves undergo modification due to changes in the thermal expansion properties of the composite. Non-uniform spatial distributions of matrix cracking can contribute to thermal stresses, just as non-uniform temperature distributions do.

The tight connection between matrix cracking and thermal stress loading motivates the study in this paper. This initial study is limited to the thermal expansion behaviour of unidirectional fibre-reinforced composites as influenced by matrix cracking and fibre sliding. Some earlier work on this general problem[1,2] was not limited to unidirectional reinforcement, but was focused on the influence of matrix cracking unaccompanied by sliding. It will be seen that sliding has an important and sometimes dominant effect on thermal expansion behaviour.

Most ceramic fibre/matrix systems of interest to date have fibres whose coefficients of thermal expansion (CTEs) are smaller than those of the matrix, in some cases by as much as a factor of two. As a consequence, at all temperatures below the 'bonding' temperature, the matrix sustains a residual tension parallel to the fibres and the fibre–matrix interface is subject to a residual compression. When matrix cracking is accompanied by fibre sliding, as it often is, the interface remains closed and friction impedes the sliding process. For composites whose fibres have smaller thermal expansivity than their matrix, matrix cracking lowers the effective CTEs relative to values for the uncracked composite. In the extreme, matrix cracking and sliding can reduce the composite CTE in the direction parallel to the fibres to a level characteristic of that of the fibre.

In presenting the results of this study, it will be convenient to focus on systems where the fibre expansivities are less than those of the matrix, although the formulae

* To whom correspondence should be addressed

listed for cases involving no sliding apply equally well to the opposite case, assuming the matrix cracks are open. The fibres are assumed to have transversely isotropic elastic moduli and thermal expansivities, while the matrix is taken to be isotropic. The effective properties of the composite are transversely isotropic about the fibre direction. Results for the thermal expansion behaviour of the composite will be presented as a function of the spacing of the matrix cracks d, the extent of the sliding zone l on either side of the matrix crack, and the friction stress τ acting across the fibre–matrix interface in the sliding zone. Debonding, *per se*, is not addressed, although a framework for analysing thermally driven debonding will be presented.

The cylindrical cell shown in *Figure 1* will be employed to model the composite. The cell has previously been used by a number of researchers to study the tensile stress–strain behaviour of unidirectional fibre-reinforced composites, both with and without matrix cracks. Motivation for the cylindrical cell approximation is included in *Figure 1*. The doubly periodic geometry of hexagonally arranged fibres with equally spaced matrix cracks extending across the entire composite can be approximated by a single cylindrical cell with special boundary conditions discussed later. This cell will be analysed at several levels of approximation, including shear-lag and finite element analyses. The present paper draws heavily on earlier work on this same cell model and should be regarded as the third in a sequence of papers which includes those by Hutchinson and Jensen[3], hereafter referred to as HJ, and He, Wu, Evans and Hutchinson[4], referred to as HWEH.

The paper is organized in a way which presents results in increasing order of complexity. Specifically, after a description of the problem to be solved in the next section, the thermal expansion coefficients of the perfectly bonded, uncracked composite are presented and compared with previous results, both experimental and theoretical. These provide the reference against which changes in behaviour due to matrix cracking and fibre sliding can be compared. Next, results will first be presented for the expansion coefficients for the composite with matrix cracks unaccompanied by any sliding. These results will then be extended to account for the effect of frictionless sliding along debonded portions of the fibre–matrix interface. Finally, the effect of a frictional sliding resistance τ will be considered. With friction, the behaviour of the composites becomes rather complicated, with hysteresis accompanying thermal cycling. It will be necessary to focus on a few specific aspects of the behaviour, and we have chosen to emphasize the role of friction in either suppressing sliding in a given thermal cycle, or, at the other extreme, in permitting near-frictionless sliding. In particular, with $\Delta\alpha$ as the measure of the thermal expansivity mismatch and ΔT as the amplitude of the temperature cycle, we identify limiting values of the non-dimensional parameter $\tau/(E_m\Delta\alpha\Delta T)$ which ensure that either almost no sliding occurs or that extensive sliding occurs. Results for an effective CTE for thermal cycling as dependent on this

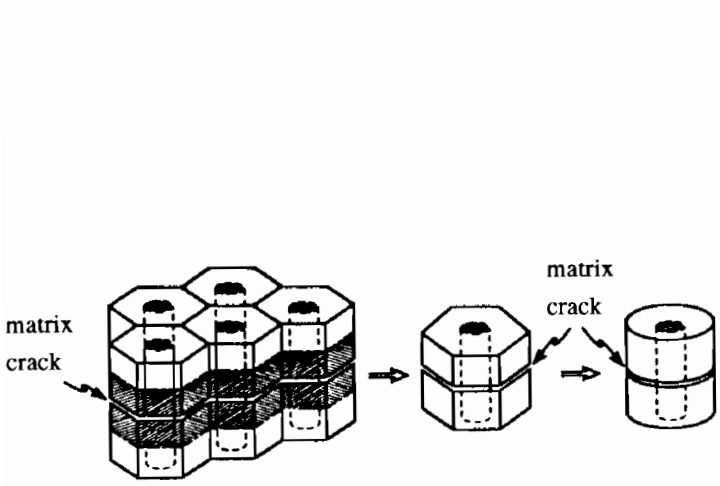

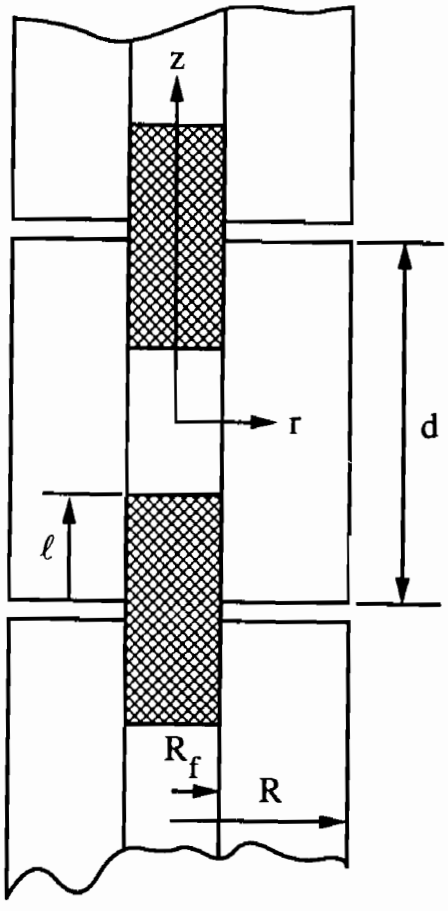

Figure 1 A cylindrical cell representation of a unidirectionally reinforced fibre/matrix composite containing a uniformly distributed, parallel array of transverse matrix cracks. The shaded areas represent the portions of the fibre–matrix interface that have debonded

non-dimensional parameter and on the density of matrix cracks will also be given.

STATEMENT OF THE PROBLEMS

Consider the composite in its current state at temperature T, as modelled in *Figure 1*. The composite has previously experienced matrix cracking and currently has a distribution of equally spaced matrix cracks a distance d apart. Both perfectly bonded and debonded fibre–matrix interfaces will be treated in the analyses to follow. Now imagine the composite undergoes a uniform temperature change from T to $T + \Delta T$. In the subsequent sections of the paper, we shall consider the following problems, all posed for the cylindrical cell model:

- axial and transverse CTEs of the uncracked composite;
- CTEs for cracked composites with either perfect bonding or with frictionless sliding along previously debonded portions of the interface; and
- overall strain changes due to ΔT for cracked composites and frictional sliding along previously debonded portions of the fibre–matrix interface, with emphasis on hysteresis effects for the cyclic variations of ΔT. Effective CTEs for thermal cycling.

Written in cylindrical polar coordinates (r, θ, z) with the z-axis coincident with the axis of the fibre, the general relation between strains and stresses for axisymmetric deformations of a linear transversely isotropic fibre is

$$\varepsilon_r = (\eta\sigma_r - \nu_r\eta\sigma_\theta - \nu_f\sigma_z)/E_f + \lambda\alpha_z^f\Delta T \quad (1a)$$

$$\varepsilon_\theta = (\eta\sigma_\theta - \nu_f\sigma_z - \nu_r\eta\sigma_r)/E_f + \lambda\alpha_z^f\Delta T \quad (1b)$$

$$\varepsilon_z = (\sigma_z - \nu_f\sigma_r - \nu_f\sigma_\theta)/E_f + \alpha_z^f\Delta T \quad (1c)$$

$$\gamma_{rz} = \tau_{rz}/G_f \quad (1d)$$

where $\eta \equiv E_f/E_r$ is the ratio of the longitudinal Young's modulus of the fibre relative to that in the transverse direction, $\lambda \equiv \alpha_r^f/\alpha_z^f$, and where α_z^f and α_r^f are axial and radial CTEs of the fibre. In general, $G_f \neq E_f/2(1+\nu_f)$. The stress–strain law for the linearly elastic, isotropic matrix with Young's modulus E_m and Poisson's ratio ν_m is

$$\varepsilon_r = [\sigma_r - \nu_m(\sigma_\theta + \sigma_z)]/E_m + \alpha_m\Delta T \quad (2a)$$

$$\varepsilon_\theta = [\sigma_\theta - \nu_m(\sigma_z + \sigma_r)]/E_m + \alpha_m\Delta T \quad (2b)$$

$$\varepsilon_z = [\sigma_z - \nu_m(\sigma_r + \sigma_\theta)]/E_m + \alpha_m\Delta T \quad (2c)$$

$$\gamma_{rz} = \tau_{rz}/G_m \quad (2d)$$

where α_m is the CTE of the matrix and $G_m = E_m/2(1+\nu_m)$.

Let α_z^0 and α_r^0 denote the longitudinal and transverse CTEs of the uncracked composite (which is also transversely isotropic). In the presence of matrix cracking coupled with *frictionless sliding* over all, or a portion of, the interface, the effective longitudinal and transverse CTEs of the composite, α_z and α_r, are defined by

$$\bar{\varepsilon}_z = \alpha_z\Delta T \qquad \bar{\varepsilon}_r = \alpha_r\Delta T \quad (3a,b)$$

where $\bar{\varepsilon}_z$ and $\bar{\varepsilon}_r$ are overall strains, defined below, induced by temperature change ΔT when no mechanical loading is applied. Analytical predictions for both α_z^0, α_r^0, and α_z, α_r based on the cylindrical cell model will be given in the sections to follow. When frictional effects are important, the overall strain changes are not linearly dependent on ΔT. It will then be necessary to consider histories of $\Delta\bar{\varepsilon}_z$ and $\Delta\bar{\varepsilon}_r$ as functions of temperature changes.

The origin of the cylindrical coordinates is taken to be at the centre of the cell, with $(z = \pm d/2,\ R_f \leq r \leq R)$ representing the two crack surfaces. Debonding, if present, is taken to occur over a cylindrical portion of the interface, extending a distance l on either side of each matrix crack surface. Thus, $l = 0$ represents the case of no debonding, while full debonding has occurred when $l = d/2$. The debonded region of the interface is assumed to have formed previously and is assumed to remain closed under the conditions assumed here where the CTE of the fibre is less than that of the matrix. If friction is present, the resistance to sliding between fibre and matrix will be characterized by a constant friction stress τ acting over the zone where sliding is currently taking place. The extent of the current sliding zone on either side of the matrix crack is denoted by L, which is necessarily embedded within the debonded region $(L \leq l)$.

It will be convenient to treat the solution to the cell model as the sum of two parts as depicted in *Figure 2*. The first part, in *Figure 2b*, is the perfectly bonded cell of infinite extent in the axial direction subject to the temperature change ΔT, measured from the reference temperature T_0 where all residual stresses vanish. The tractions on the outer cylindrical surface of the cell are zero and the cell is free to expand or contract in the axial direction. This is a classical Lame-type problem with axial stress component in the fibre, σ_f^T, and matrix, σ_m^T, given by

$$\sigma_f^T = -(1-\rho)\sigma_m^T/\rho = -a_2E_m\Delta\alpha\Delta T \quad (4a)$$

where throughout the paper the CTE mismatch is defined by

$$\Delta\alpha \equiv \alpha_z^f - \alpha_m \quad (4b)$$

The coefficient a_2 depends on the constituent parameters of the fibre and matrix and on the fibre volume fraction $\rho = (R_f/R)^2$. Formulae for this coefficient, as well as others which follow denoted by a_i, b_i and c_i, can be found in HJ. They will not be repeated here.

The second part of the solution to the cell model is depicted in *Figure 2c*. The matrix crack faces at $z = \pm d/2$ are subject to a normal stress $-\sigma_m^T$. By symmetry, the vertical displacement of the fibre at $z = \pm d/2$ is uniform such that the average axial stress in the fibre is $-\sigma_f^T$. The shear traction vanishes everywhere on $z = \pm d/2$. If debonding has occurred and if there is no friction, then the interface above $z = d/2-l$ (and below $z = -d/2+l$) is held closed with $\sigma_{rz} = 0$. If friction is present and if the current sliding zone is above $z = d/2-L$ (and below $z = -d/2+L$), then $\sigma_{rz} = \pm\tau$ within the sliding zones, depending on the sense of the sliding. The condition for determining the instantaneous value of L, assuming $L < l$, is the requirement that the magnitude of the shear stress on the interface just outside the sliding zone be less than or equal to τ. This can be expressed as a Dugdale-type condition which will be given later. When $L = l$, the sliding zone is taken to be fixed since additional debonding is not considered in this paper. The boundary conditions on the lateral sides of the cell in *Figure 2c* are specified by requiring the shear traction to vanish and the radial displacement component to be uniform over the outer surface such that the radial stress averaged over this surface vanishes. This type of boundary condition mimics the constraint expected for

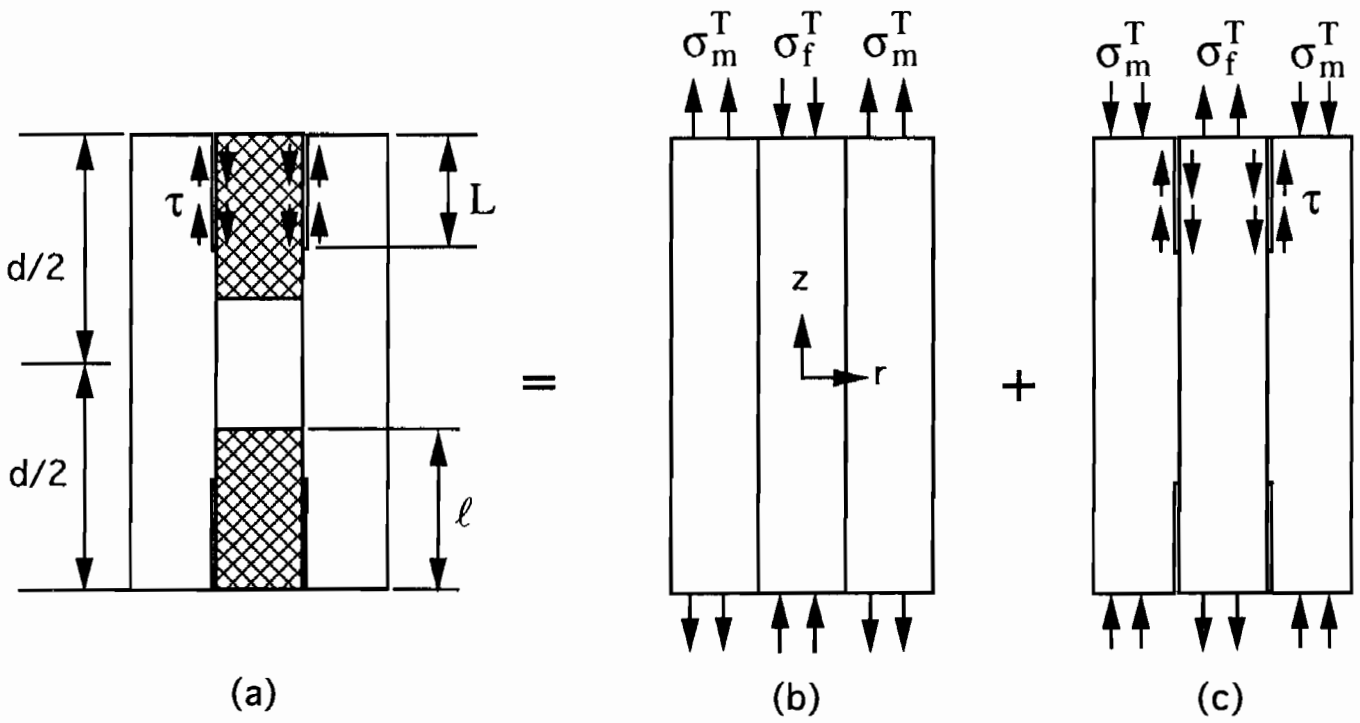

Figure 2 Conventions and superposition solution schematics for axisymmetric cell model

identical interacting cells and was previously used in HJ, in Pagano and Brown[5], and HWEH.

The full solution to the cell model is the linear superposition of the two parts specified above. Note that the full solution is characterized by the constrained outer boundary condition just mentioned because the solution in *Figure 2b* satisfies it trivially. The overall composite strains, $\bar{\varepsilon}_z$ and $\bar{\varepsilon}_r$, are defined using *Figure 1* as the axial displacement difference between sections at $z = d/2$ and $z = -d/2$ divided by d and the radial displacement at $r = R$ divided by R, respectively. Approximate closed-form solutions will be obtained for the problem in *Figure 2c* using a shear-lag analysis, which is improved upon with the aid of some finite element results. The problem has a large number of parameters, thereby highlighting the importance of accurate, closed-form approximations for assessing trends in the parametric dependences of the composite CTEs.

CTEs OF UNCRACKED COMPOSITES

Many analytical models exist for the prediction of the CTEs for uncracked unidirectional composites. Some of these are critically reviewed and compared with experimental measurements by Bowles and Tompkins[6]. For the most part, large discrepancies between the predicted values of the transverse CTE and the test data are observed, except for the model of Rosen and Hashin[7], which is identical to the present model. Bowles and Tompkins also conducted finite element calculations for two cell geometries, including a doubly periodic hexagonal pattern, and showed that their results were in good agreement with the experimental values and with the Rosen–Hashin analysis. This solution provides the reference for the present investigation. Presented below is a somewhat more compact set of equations for CTEs predicted by the cylindrical cell model.

Using the results in HJ for the Lame problem in *Figure 2b* together with the results for the radial displacement at the surface of the cell, one obtains the CTEs of the uncracked composite from the definitions in equations (3) as

$$\alpha_z^0 = \rho\alpha_z^f + (1-\rho)\alpha_m - \rho\Delta\alpha \times\left[a_2\left(\frac{E_m}{E_f}-1\right)+2a_4\left(\nu_m-\nu_f\frac{E_m}{E_f}\right)\right] \quad (5a)$$

$$\alpha_r^0 = \rho\alpha_r^f + (1-\rho)\alpha_m - \rho\Delta\alpha \times\left[a_2\left(\nu_m-\nu_f\frac{E_m}{E_f}\right)+2a_4\left(\zeta_f\frac{E_m}{E_f}-1+\nu_m\right)\right] \quad (5b)$$

where new symbols are defined in the Notation and the non-dimensional coefficients a_2 and a_4 are given in HJ. For isotropic fibres with $\lambda = \eta = 1$ and for systems with $\nu_f = \nu_m = \nu$, equations (5a) and (5b) simplify to

$$\alpha_z^0 = \alpha_m + \frac{\rho E_f}{E}\Delta\alpha \quad (6a)$$

$$\alpha_r^0 = (1-\rho)\alpha_m + \rho\alpha_f - \Delta\alpha \times\frac{\rho(1-\rho)(E_f-E_m)[\nu E_f+(3\nu-2)E]}{E[E_f+(1-2\nu)E]} \quad (6b)$$

where $E = (1-\rho)E_m + \rho E_f$ is the modulus of the uncracked composite in the axial direction.

The predictive capability of equations (5) is illustrated in *Figure 3*, where the NASA test data for several material systems at room temperature are also included for comparison. The material systems considered are T300/934 (graphite/epoxy), P75/934 (graphite/epoxy), P100/2024 (graphite/aluminium), HMS/borosilicate (graphite/glass) and C6000/PMR 15 (graphite/polyimide). The properties of the constituents are tabulated

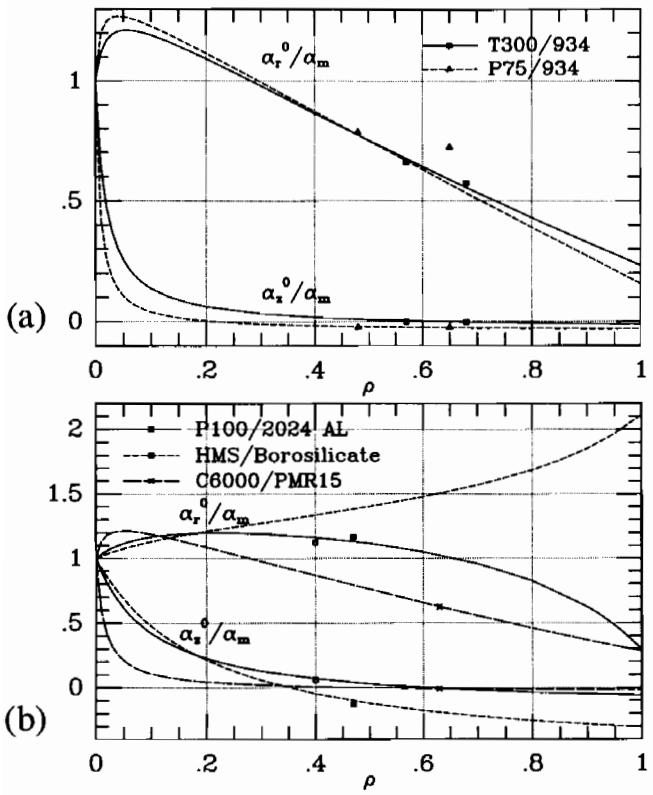

Figure 3 Cell model predictions and NASA test data for axial and transverse CTEs of uncracked unidirectional composites: (a) T300/934 and P75/934; (b) P100/2024, HMS/borosilicate and C6000/PMR 15

in Bowles and Tompkins[6]. *Table 1* summarizes the experimentally measured values and the predicted values from equations (5).

CTEs OF CRACKED COMPOSITES IN THE ABSENCE OF FRICTION

Perfect bonding

For perfectly bonded fibre–matrix interfaces, the effective CTEs of a cracked unidirectional composite with fixed crack spacing d have been obtained in the Appendix with the aid of the shear-lag analysis of the cylindrical cell. These results are approximate due to the one-dimensional nature of the shear-lag analysis. Nonetheless, they reveal the important functional dependence of the crack-affected CTEs on constituent properties and pertinent geometrical parameters. Results obtained by the finite element method (FEM) have been used to improve the approximations introduced in the shear-lag analysis. Details of the numerical FEM scheme pertaining to the present cell model are similar to those reported in HWEH.

For well separated matrix cracks (i.e. $d/R_f > 3$, see discussion below), interaction between cracks is small and the solutions for α_z and α_r are given by

$$\alpha_z = \alpha_z^0 + D_1^0 \frac{\Delta\alpha E_m \rho a_2}{E(1 - a_1\rho)} \frac{R_f}{d} \tag{7a}$$

$$\alpha_r = \alpha_r^0 + \xi D_1^0 \frac{E_f}{E_m} \frac{\Delta\alpha E_m \rho a_2}{E(1 - a_1\rho)} \frac{R_f}{d} \tag{7b}$$

Here, ξ is a non-dimensional coefficient defined by

$$\xi = \rho\left[\left(\nu_m - \nu_f \frac{E_m}{E_f}\right) + b_1\left(\zeta_f \frac{E_m}{E_f} - 1 + \nu_m\right)\right] \tag{7c}$$

The dimensionless coefficient D_1^0 is the same as that introduced in HWEH to account for the increased compliance of the composite under axial load due to (dilute) matrix cracking without debonding. It was computed as a function of ρ and E_f/E_m by a finite element analysis in HWEH and is included here in *Figure 4*. When the fibre is isotropic with $\lambda = \eta = 1$ and $\nu_m = \nu_f = \nu$, equations (7) can be further reduced to give

$$\alpha_z = \alpha_z^0 + \Delta\alpha D_1^0 \frac{\rho H R_f}{(1 - \rho)d} \tag{8a}$$

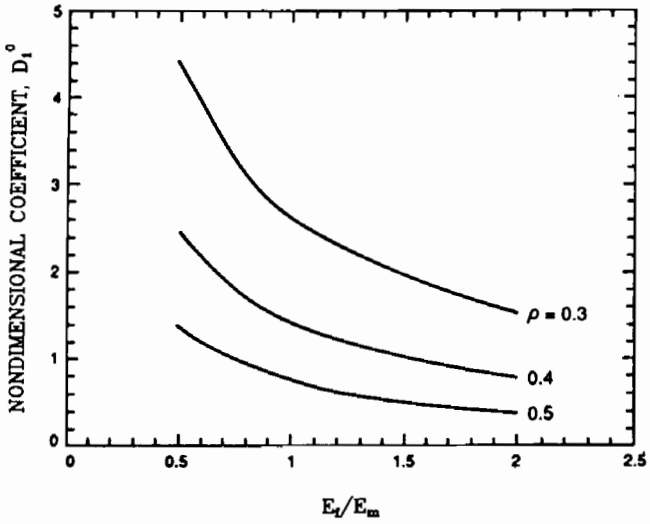

Figure 4 Numerical results for dimensionless coefficient D_1^0

Table 1 Comparison between experimentally measured and predicted CTEs for several uncracked composite systems at room temperature

Material system	ρ	α_z^0 (10^{-6} °C^{-1}) (measured)	α_r^0 (10^{-6} °C^{-1}) (measured)	α_z^0 (10^{-6} °C^{-1}) (predicted)	α_r^0 (10^{-6} °C^{-1}) (predicted)
T300/5208	0.68	–0.167	37.11	–0.135	35.93
T300/934	0.57	–0.003	42.7	0.235	43.61
P75/934	0.48	–1.546	50.77	–1.355	50.07
P75/930	0.65	–1.583	46.64	–1.660	36.80
P75/CE339	0.54	–1.501	69.72	–1.263	62.84
P100/2024 Al	0.63	–0.312	32.98	–0.274	33.19
C6000/PMR 15	0.47	–0.609	5.559	–0.478	6.584
HMS/borosilicate	0.40	2.118	38.41	2.405	39.71

$$\alpha_r = \alpha_r^0 + \Delta\alpha D_1^0 \frac{\nu(1+\nu)\rho^2 H R_f E_f (E_f - E_m)}{(1-\rho)E_m[1+\nu)E_f + (1-\nu)E]d} \quad (8b)$$

where

$$H = \frac{(1-\rho)E_f(E_f+E)}{E[E_f + (1-2\nu)E]} \quad (8c)$$

For crack spacings smaller than about three times the fibre radius, the dependence of the effective CTEs on the crack density parameter, R_f/d, becomes non-linear due to interaction between cracks, with α_z approaching (approximately) α_z^f when $d \to 0$. The approximate analysis of the Appendix gives the following formulae for α_z and α_r, which are valid over the whole range of d/R_f:

$$\alpha_z = \alpha_z^0 + D_1 \frac{\Delta\alpha E_m \rho a_2 R_f}{Ed(1 - a_1\rho)} \quad (9a)$$

$$\alpha_r = \alpha_r^0 + \xi D_1' \frac{\Delta\alpha E_m \rho a_2 R_f}{Ed(1 - a_1\rho)} \quad (9b)$$

where

$$D_1 = D_1^0 \tanh\left(\frac{Sd}{D_1^0 R_f}\right) \quad D_1' = D_1^0 \frac{E_f}{E_m} \tanh\left(\frac{Sd}{D_1^0 R_f}\right) \quad (10)$$

Here, $S = (1 - a_1\rho)(1-\rho)/(\rho a_2)$ is the slope of the curve of D_1 *versus* d/R_f when d/R_f is small such that $\alpha_z = \alpha_z^f$ for d=0. For isotropic fibres and $\nu_f = \nu_m$, $S = (1-\rho)^2 E_m/(\rho EH)$.

We note in passing that there is a close connection between the present problem for the effect of matrix cracking on the CTEs and the problem for the effect of matrix cracks on the increase in compliance of the composite under axial load. Using the above results and the connection between the two problems detailed in HWEH, one can obtain the following companion result for the axial modulus of the cracked composite:

$$E_c = E\left(1 + D_1 \frac{R_f}{d}\right)^{-1} = E\left[1 + D_1^0 \frac{R_f}{d} \tanh\left(\frac{S}{D_1^0}\frac{d}{R_f}\right)\right]^{-1} \quad (11)$$

This result is reminiscent of the solution of Laws and Dvorak[8] for the Young's modulus $\bar{E}_c$ of a cross-ply laminate as a function of the transverse matrix crack spacing d, which reads

$$\bar{E}_c = E_0\left[1 + \frac{cE_t}{2bE_l}\frac{c}{\zeta d}\tanh\left(\zeta\frac{d}{c}\right)\right]^{-1} \quad (12)$$

where the shear-lag parameter is $\zeta = \zeta_1 (bE_l + cE_t)/(2bE_lE_t)$. Here, b and E_l are respectively the thickness and modulus of the 0° ply, $2c$ and E_t are respectively the thickness and modulus of the 90° ply, E_0 is the modulus of the uncracked laminate and ζ_1, like D_1^0, is a semi-empirical parameter to be determined from either experiments or numerical solutions.

Selected predictions from equations (9) are shown in *Figure 5*, together with results from a detailed FEM analysis of the cell model. In this figure, both fibre and matrix are taken to be isotropic with $\lambda = \eta = 1$, $\rho = 0.3$, $\nu_f = \nu_m = 0.3$, $E_f/E_m = 2$ and $\alpha_z^f/\alpha_m = 0.5$, representative of some ceramic matrix composites. Several features seen in *Figure 5* deserve comment, in addition to the general agreement between the predictions of the approximate formulae (9) and the FEM results. First, matrix cracking has little effect on the radial CTE. Second, there is little difference between the dilute prediction for the axial CTE, α_z, from equation (7a) and the prediction from equation (9a) as long as $d/R_f > 3$. The two predictions diverge significantly for $d/R_f < 2$. Dilute results will often be adequate since crack spacings in a unidirectional composite seldom fall below $3R_f$. When the crack spacing d approaches zero, equation (9a) has been constructed such that α_z approaches the CTE of the fibre, α_z^f, and this limit is noted in the figure. This limit is slightly in error due to a Poisson interaction in the radial direction between the fibre and matrix which still persists even when the crack density becomes large, and whch is not accounted for by the approximate formula (9a). This effect can be seen in the difference between the predictions of equation (9a) and the FEM results in *Figure 5*. The axial CTE is slightly larger than α_z^f as the crack density becomes large. Lastly, it can be noted that d/R_f can be regarded as a 'large' crack density when $d = R_f$ in the sense that any higher density produces relatively little further change in the CTEs. Thus, the transition range of crack densities, from dilute to effectively fully cracked, is roughly $1/3 < R_f/d < 1$.

Figure 6 shows how the axial CTE of the composite discussed above depends on E_f/E_m (*Figure 6a*) and on ρ (*Figure 6b*). In these plots α_z is normalized by the axial CTE of the uncracked composite α_z^0, which is a function of both E_f/E_m and ρ. The comments made above about the departure from the dilute predictions and the transition to the CTE of the fibre remain pertinent.

Partially or fully debonded interface with frictionless sliding

Frictionless sliding over debonded portions of the fibre–matrix interface further relaxes the constraint of

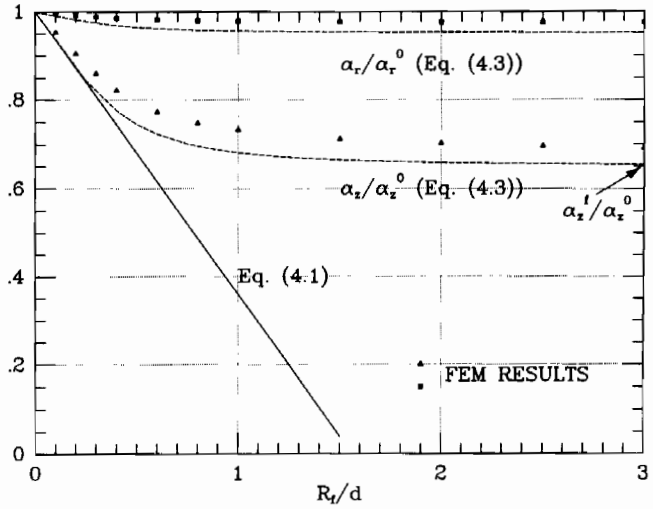

Figure 5 Cell model predictions and FEM results for normalized axial and transverse CTEs, α_z/α_z^0 and α_r/α_r^0, as functions of normalized crack density R_f/d. The constitutive parameters used are $\lambda = \eta = 1$, $\rho = 0.3$, $\nu_f = \nu_m = 0.3$, $E_f/E_m = 2$ and $\alpha_z^f/\alpha_m = 0.5$

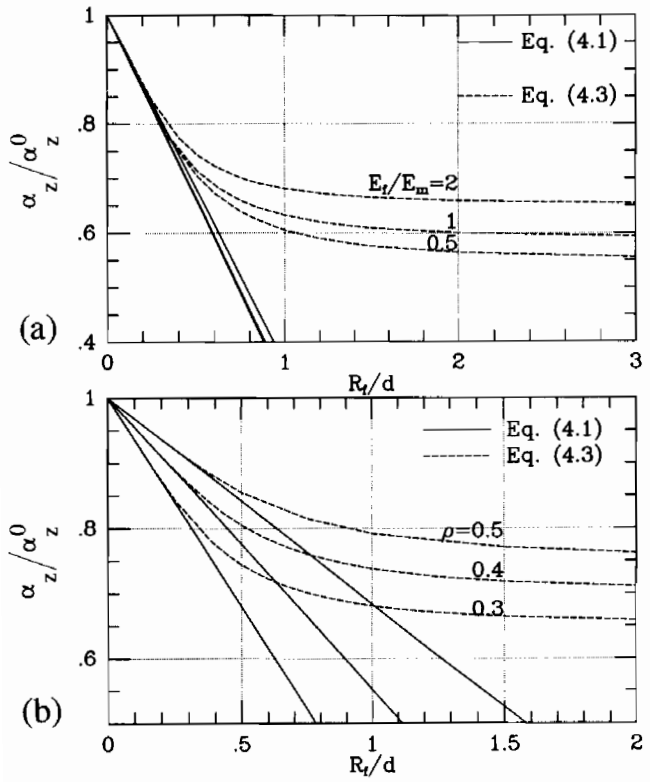

Figure 6 Predicted axial CTE as a function of crack density for varying values of: (a) E_f/E_m and (b) fibre volume fraction ρ. The constitutive parameters are the same as those listed in *Figure 5*

the matrix on the fibres under a temperature change. For a given matrix crack spacing d and a *fixed* debond length l, the effective CTEs of the composite, α_z and α_r, are still formally given by equations (9) (relevant background is given in HWEH). Now, however, there are extra contributions to D_1 and D_1^r arising from frictionless sliding:

$$D_1 = D_1^0\left(1-\frac{2l}{d}\right)\tanh\left(\frac{S(d-2l)}{D_1^0 R_f}\right)+8\rho\frac{E}{E_m}\frac{l}{R_f}c_1^2 \quad (13)$$

$$D_1^r = D_1^0\left(1-\frac{2l}{d}\right)\frac{E_f}{E_m}\tanh\left(\frac{S(d-2l)}{D_1^0 R_f}\right)+\frac{2(1-a_1\rho)El}{E_m\rho R_f} \quad (14)$$

The first terms in each of these equations correspond to the contribution from matrix cracking alone, as in equations (10), but modified to be zero when the interface becomes fully debonded at $l = d/2$. The second term in each expression is the contribution from the debonded region of the interface. This contribution is obtained from the HJ solutions (see also HWEH). The coefficient c_1 in expression (13) is given in HJ for two sets of boundary conditions, termed type I and II, and was derived for the limiting case $l << d$, or, effectively, $d = \infty$. Type I models a cell with zero radial stress everywhere on the outer surface of the cell (i.e. on $r = R$). Type II conditions enforce the same uniform radial displacement on the outer surface of the cell that occurs in the unbonded region. When $l << d$, this is equivalent to requiring that the *average* radial stress on the outer surface of the cell is zero, just as posed for the cell in *Figure 1*. Within the level of approximation employed in the present paper, type II conditions for c_1 should be used when $l << d$ and type I conditions used when $l \cong d/2$. Neither of the two conditions applies strictly for a partially bonded interface when l is of the order of $d/2$. In any case, the difference between the two values of c_1 is generally quite small, with the difference vanishing altogether when there is no elastic mismatch between the fibre and the matrix. It is felt that the extra complication involved in more accurately characterizing this aspect of the partially debonded regime is not worth the effort.

If the fibre is isotropic ($\lambda = \eta = 1$) and if $\nu_f = \nu_m = \nu$, a useful intermediate level of approximation to equations (13) and (14) is obtained under the assumption that the matrix crack interaction is small (i.e. $d > 3R_f$) such that tanh() ≈ 1. Then, as a further approximation, using type I conditions in HJ to evaluate c_1 in equation (13), one obtains from equations (9)

$$\alpha_z = \alpha_z^0 + \Delta\alpha\frac{\rho H R_f}{(1-\rho)d}\left[D_1^0\left(1-\frac{2l}{d}\right)+\frac{(1-\rho)E_m}{\rho E_f\chi^2}\frac{2l}{R_f}\right] \quad (15a)$$

$$\alpha_r = \alpha_r^0 + \Delta\alpha\frac{\nu(1+\nu)\rho^2 H E_f(E_f-E_m)R_f}{(1-\rho)E_m[(1+\nu)E_f+(1-\nu)E]d} \times\left[D_1^0\left(1-\frac{2l}{d}\right)+\frac{(1-\rho)}{\rho}\frac{2l}{R_f}\right] \quad (15b)$$

where

$$\chi = \sqrt{\frac{(1+\nu)E_f+(1-\nu)E}{(1+\nu)[E_f+(1-2\nu)E]}} \quad (15c)$$

When the interface is fully debonded with $l = d/2$, the first terms in equations (13) and (14) vanish altogether. Then, equations (9) predict that the effective CTEs of the composite with free-sliding interfaces are independent of the matrix crack density according to

$$\alpha_z = \alpha_z^0 + 4a_2\rho^2 c_1^2\frac{\Delta\alpha}{1-a_1\rho} \qquad \alpha_r = \alpha_r^0 + \xi a_2\Delta\alpha \quad (16a,b)$$

As discussed above, the value of c_1 for type I boundary conditions is now applicable. Specializing further to the case of an isotropic fibre ($\lambda = \eta = 1$) and $\nu_f = \nu_m = \nu$, one finds from equations (15)

$$\alpha_z = \alpha_z^0 + \Delta\alpha\frac{E_m H}{E_f\chi^2} \quad (17a)$$

$$\alpha_r = \alpha_r^0 + \Delta\alpha\frac{\nu(1+\nu)\rho H E_f(E_f-E_m)}{(1-\rho)E_m[(1+\nu)E_f+(1-\nu)E]} \quad (17b)$$

The predictions based on equations (9), (13) and (16) are illustrated in *Figure 7* as plots of α_z/α_z^0 *versus* R_f/d for five values of normalized debond length l/R_f. Corresponding curves for α_r/α_r^0 will not be shown since there is relatively little change in the radial component of the CTE from the value for the uncracked composite. These predictions are for the same choices of parameters used in the earlier examples, i.e. $E_f/E_m = 2$, $\rho = 0.3$, $\nu_f = \nu_m = 0.3$, $\alpha_z^f/\alpha_m = 0.5$ and $\lambda = \eta = 1$. The horizontal line in *Figure 7* is the result for the fully debonded

composite and is independent of the density of matrix cracks. Note that the fully debonded, free-sliding composite has a CTE which is slightly *less* than that of the fibre itself, $\alpha_z/\alpha_z^f \cong 0.88$ in the present case. This seemingly anomalous result is a consequence of the Poisson interaction between the fibre and the matrix, together with the fact that the fibre–matrix interface remains closed due to residual stresses. It is brought out most clearly when equation (17a) is further specialized to the case with no elastic mismatch ($E_f = E_m$) giving $\alpha_z = \alpha_z^f + \nu\lambda(1-\rho)\Delta\alpha$, which is clearly less than α_z^f since $\Delta\alpha$ is negative. Under a temperature decrease, for example, the resulting *increase* in the radial stress component acting across the fibre–matrix interface produces an axial Poisson *contraction* in the fibre, slightly decreasing its axial expansion. This small contribution would be absent if the interface lost contact.

A curve in *Figure 7* for a given value of normalized debond length intersects the horizontal line when the fibre becomes fully debonded, i.e. $l = d/2$. Using the result for the perfectly bonded case ($l/R_f = 0$) as reference, one can see that debonding with frictionless sliding has a significant effect on reducing the axial CTE of the composite to values comparable to that of the fibre. Without sliding, a relatively high density of matrix cracks is needed to produce a substantial drop in the CTE. The combination of matrix cracking and sliding has a substantially larger effect. In the next section, the role of frictional sliding resistance will be considered.

THERMAL EXPANSION BEHAVIOUR OF CRACKED COMPOSITES WITH FRICTIONAL SLIDING

Frictional sliding complicates the thermal expansion behaviour of a cracked composite. When frictional sliding is important, the composite strain no longer varies linearly with changes in temperature. The zone of frictional sliding varies with temperature, and hysteresis effects will occur under cyclic thermal histories. In the absence of friction, the axial CTE is bracketed by the value of that for the uncracked composite, α_z^0, and a value which, at its lowest, is only slightly less than that of the fibre, α_z^f. The extent of matrix cracking and sliding determines where between these brackets the CTE lies.

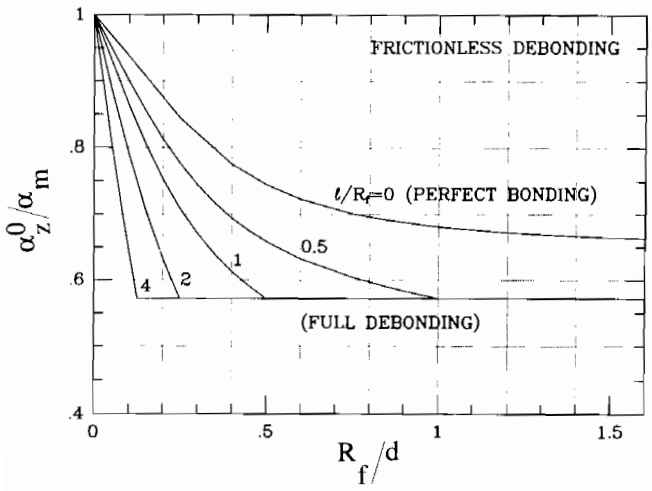

Figure 7 Effect of frictionless debonding on the axial CTE of a cracked unidirectional composite. The constitutive parameters are the same as those listed in *Figure 5*

The sliding contribution to strain increments will be reduced by friction. It is this effect which is quantified in this section. Results obtained here will emphasize cyclic thermal loading, but a framework for analysing strain changes under general thermal histories will be presented.

For completeness, consider a temperature history such as that shown in *Figure 8a*, where T starts at the 'bonding' temperature T_0, with the composite in a state with no residual stress. Then the temperature drops to T_A, and thereafter cycles 'steadily' between T_A and T_B with $T_A < T_B < T_0$. Assume that there is a fixed matrix crack spacing d, that the debonding energy of the fibre can be neglected, and that the friction stress τ is independent of T and undiminished by repeated reversed sliding. Starting at T_0, as in *Figure 8a*, simplifies the discussion, but is not essential. For a given spacing of matrix cracks d and interface debonding length l, it can be shown that, once a full cycle of such a steady-cycle history has taken place, there is no influence of the prior thermal history on the subsequent *incremental* behaviour of the composite. The axial strain of the composite and the length L of the current zone of sliding varies with time as sketched qualitatively in parts *b* and *c* of *Figure 8*. The example illustrated applies to a case where the sliding zone does not engulf the full interface (i.e. $L < d/2$). A cross-plot of axial strain *versus* temperature is shown in *Figure 8d*, showing the fact that the strain cycles in a hysteresis loop as soon as the 'steady' thermal cycle is in effect. Three reference slopes are indicated in *Figure 8d*: that of the uncracked composite, that of the cracked composite with no sliding, and that of the cracked, freely-sliding composite. As T increases from T_A, the initial slope coincides with that of the cracked composite with

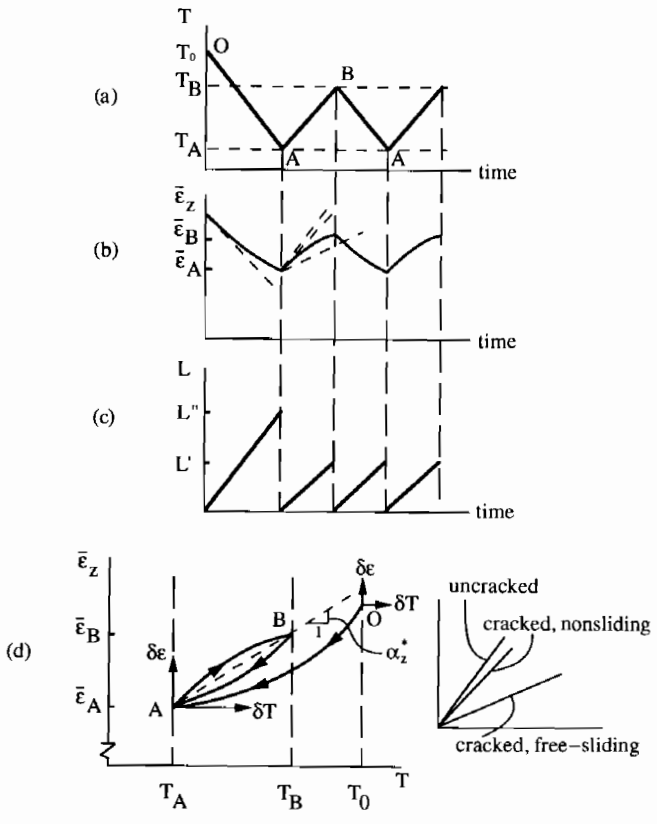

Figure 8 Schematic behaviour due to thermal cycling in the presence of frictional sliding

no sliding; but as T increases, the sliding region grows and the slope drops. The slope attains that of the freely-sliding composite if L reaches $d/2$. After T reverses at T_B and starts to drop, the instantaneous slope again starts as that of the cracked composite with no sliding and progressively drops towards that of the freely-sliding composite. The average strain change associated with the closed hysteresis loop can be characterized by an effective CTE, α_z^*, defined such that $\bar{\varepsilon}_B - \bar{\varepsilon}_A = \alpha_z^*(T_B - T_A)$, as indicated in *Figure 8d*. This effective CTE will approach that of the cracked, non-sliding composite if friction effects are large, and will approach that of the cracked, free-sliding composite if friction effects are small.

Conditions for determination of length L *of current sliding zone and incremental strain changes due to temperature increment*

To limit the complexity of this study, assume that the matrix crack spacing d is fixed and that either: (1) the fibre–matrix interface has been fully debonded at a prior time in the loading history, or (2) the fibre–matrix interface debond toughness can be neglected. Determination of the length L of the current sliding zone requires information from the cell model in *Figure 2* about the mode II stress intensity factor K_{II} at the end of the sliding region. If the interface just ahead of the sliding zone were not debonded, K_{II} would have to attain the debond intensity toughness if the zone were to increase in size. For either prior debonding or negligible debond toughness, the condition for determining the instantaneous position of the end of the sliding region is $K_{II} = 0$. Given τ acting over the portion of the interface undergoing sliding, this condition ensures that the shear stress on the interface ahead of the sliding zone falls off continuously from τ.

The analysis of straining due to cyclic thermal histories is best carried out using formulae for incremental quantities. The approach is similar in many respects to that which accounts for frictional sliding in the analysis of matrix cracking due to fatigue crack growth in composites under cyclic mechanical loads[9]. Let δT and $\delta\bar{\varepsilon}_z$ denote increments of temperature and overall longitudinal strain measured from the last point of temperature reversal, such as O, A or B in *Figure 8*. Consider the first temperature excursion in *Figure 8* starting from T_0 with the composite in the unstressed state. As T drops, L increases from zero with τ acting over the sliding zone in the sense shown in *Figure 2*. With $\delta T = T - T_0$, the cell model of *Figure 2* gives K_{II} at the end of the sliding zone and $\delta\bar{\varepsilon}_z$ and $\delta\bar{\varepsilon}_r$ measured relative to the strain at T_0 as

$$K_{II} = D_2 \frac{\Delta\alpha\delta T E_m \rho a_2 \sqrt{R_f}}{(1 - a_1\rho)} - D_4 \frac{\tau L}{\sqrt{R_f}} \tag{18}$$

$$\delta\bar{\varepsilon}_z = \alpha_z^0 \delta T + D_1 \frac{\rho a_2 R_f E_m \Delta\alpha\delta T}{E(1 - a_1\rho)d} - D_3 \frac{\tau L^2}{E R_f d} \tag{19}$$

$$\delta\bar{\varepsilon}_r = \alpha_r^0 \delta T + \xi D_1' \frac{\rho a_2 R_f E_m \Delta\alpha\delta T}{E(1 - a_1\rho)d} - \xi D_3' \frac{\tau L^2}{E R_f d} \tag{20}$$

The non-dimensional coefficients in these expressions not listed previously are taken from the cell analysis given by HWEH. They are:

$$D_2 = \sqrt{\frac{\hat{E}}{E_m}} c_1 \tag{21}$$

$$D_3 = b_2 D_3' = \left[\left(\frac{32}{3} \sqrt{\frac{2}{\pi}} \frac{\rho c_1 E}{\sqrt{\hat{E} E_m}} \sqrt{\frac{R_f}{L}} \right)^2 + \left(\frac{2 E b_2}{E_m} \right)^2 \right]^{1/2} \tag{22}$$

$$D_4 = \left\{ \left(\frac{\pi R_f}{L} \right)^2 + \left[(b_2 + b_3) \left(\frac{\hat{E}}{E_m} \right) \right]^2 \right\}^{1/4} \tag{23}$$

where the modulus quantity $\hat{E}$ is given by

$$\frac{1}{\hat{E}} = \frac{1}{2}(1 - \beta^2) \left(\frac{1 - \nu_m^2}{E_m} + \frac{1 - \nu_f^2}{E_f} \right) \tag{24}$$

and β is the second plane strain moduli mismatch parameter of Dundurs.

Imposition of $K_{II} = 0$ on equation (18) gives the sliding length as T drops from T_0 as the solution to

$$\frac{L}{R_f} = \frac{D_2}{D_4(L)} \frac{\rho a_2}{(1 - \rho a_1)} \left(\frac{E_m \Delta\alpha\delta T}{\tau} \right) \tag{25}$$

where $\delta T = T - T_0$. This relation applies as long as $L < d/2$. The current sliding zone engulfs the entire interface when L attains $d/2$, and then L remains fixed at $d/2$ until the temperature reverses at T_A. The zone length L'' at the end of the first temperature excursion in *Figure 8c* is given by the smaller of $d/2$ and the value given by equation (25) with $\delta T = T_A - T_0$. The strain changes occurring in the drop from T_0 to T_A are given by equations (19) and (20) with $L = L''$ and $\delta T = T_A - T_0$.

Straining behaviour under cyclic thermal loading

Next consider the rise in T from T_A to T_B, and now let $\delta T = T - T_A$ and measure $\delta\bar{\varepsilon}_z$ from the state at A. Equations (18)–(20) continue to apply to *increments* measured from A if τ is replaced by -2τ and as long as the length of the current sliding zone does not exceed the length (L'') of the sliding zone prior to reversal. This replacement accounts for the change in the sense in which the friction stress acts, and for the fact that 2τ represents the magnitude of the *change* in the shear stress in the sliding zone from its value prior to reversal. Thus, as T increases from T_A

$$\frac{L}{R_f} = \frac{D_2}{D_4(L)} \frac{\rho a_2}{(1 - \rho a_1)} \left(\frac{E_m \Delta\alpha\delta T}{-2\tau} \right) \tag{26}$$

and

$$\delta\bar{\varepsilon}_z = \alpha_z^0 \delta T + D_1 \frac{\rho a_2 R_f E_m \Delta\alpha\delta T}{E(1 - a_1\rho)d} + D_3 \frac{2\tau L^2}{E R_f d} \tag{27}$$

The sliding zone length L' as T attains T_B will be given by equation (26) with $\delta T = T_B - T_A$, unless $L = d/2$ at some T less than T_B in which case $L' = d/2$. That is, L' is the smaller of $d/2$ or the solution to

$$\frac{L'}{R_f} = \frac{D_2}{D_4(L')} \frac{\rho a_2}{(1 - \rho a_1)} \left(\frac{E_m \Delta\alpha (T_A - T_B)}{2\tau} \right) \tag{28}$$

(Note that it is obvious from comparing equation (28) with equation (25) that L' will never exceed L'' as long as $T_B < T_0$). The axial strain change occurring from A to B, $\delta\bar{\varepsilon}_z = \bar{\varepsilon}_B - \bar{\varepsilon}_A$, is given by equation (27) with $L = L'$ and $\delta T = T_B - T_A$.

Now consider reversal at B with T dropping from T_B. The arguments just made continue to pertain for the incremental problem. In particular, equations (18)–(20) apply if τ is replaced by 2τ, if $\delta T = T - T_B$, and if $\delta\bar{\varepsilon}_z$ is measured from B. Specifically, equations (26) and (27) apply with only a sign change on τ. It immediately follows that the sliding zone length equals L' as T attains T_A, where L' is the length given above. Moreover, the axial strain change occurring in the temperature drop from B to A is equal in magnitude and opposite in sign to that occurring on the leg of the cycle from A to B. Thus, the cycle of strain is closed, as depicted in *Figure 8*.

The effective axial CTE for the cycle, which is indicated in *Figure 8d*, is given by

$$\alpha_z^* \equiv \frac{\bar{\varepsilon}_B - \bar{\varepsilon}_A}{T_B - T_A} = \alpha_z^0 + D_1 \frac{\rho a_2 R_f E_m \Delta\alpha}{E(1 - a_1\rho)d} + D_3 \frac{2\tau(L')^2}{ER_f d(T_B - T_A)} \tag{29}$$

where L' is given by the smaller of $d/2$ or the solution to equation (28). A closed-form expression for α_z^*, which is accurate for crack spacings satisfying $d > 3R_f$ and for all but the smallest values of $E_m\Delta\alpha(T_A - T_B)/\tau$, is obtained with the aid of the following approximations. As before, the tanh( ) term in D_1 is set to 1, and the terms involving R_f/L in D_3 in equation (22) and in D_4 in equation (23) are neglected. Then when L' is eliminated from equation (29), one obtains

$$\alpha_z^* = \alpha_z^0 + \Delta\alpha H \frac{R_f}{d}\left\{\frac{\rho D_1^0}{1-\rho} + H\left[-\frac{\rho D_1^0 R_f}{2d(1-\rho)} + \left(\frac{E_m(2E_f - E)}{4E_f^2\chi^2}\right)\right]\frac{E_m\Delta\alpha(T_A - T_B)}{\tau}\right\} \tag{30a}$$

for $L' < d/2$ or (equivalently) for $E_m\Delta\alpha(T_A - T_B)/\tau < [2d/(HR_f)]$, and

$$\alpha_z^* = \alpha_z^0 + \Delta\alpha \frac{E_m}{E_f\chi^2}\left\{H - \frac{d}{R_f}\frac{E}{E_f}\frac{\tau}{E_m\Delta\alpha(T_A - T_B)}\right\} \tag{30b}$$

for $L' = d/2$ or (equivalently) for $E_m\Delta\alpha(T_A - T_B)/\tau \geq [2d/(HR_f)]$.

Figure 9a displays plots of L'/R_f *versus* $E_m\Delta\alpha(T_A - T_B)/\tau$ from equation (28) for three values of E_f/E_m with $\nu_f = \nu_m = 0.3$, $\rho = 0.3$ and $\lambda = \eta = 1$. (Again, note that $\Delta\alpha$ is negative so that $E_m\Delta\alpha(T_A - T_B)/\tau$ is positive.) A companion plot based on equations (30) for the effective axial CTE is shown in *Figure 9b* for $d/R_f = 8$. The trends in α_z^* described earlier are evident in this plot. Small values of $E_m\Delta\alpha(T_A - T_B)/\tau$ are associated with values of α_z^* which are close to the axial CTE of the cracked, non-sliding composite, while large values of this parameter result in an effective axial CTE which is close to that of the fibre. The half way point between these two limiting behaviours is roughly given by the condition that $L' = d/2$, i.e.

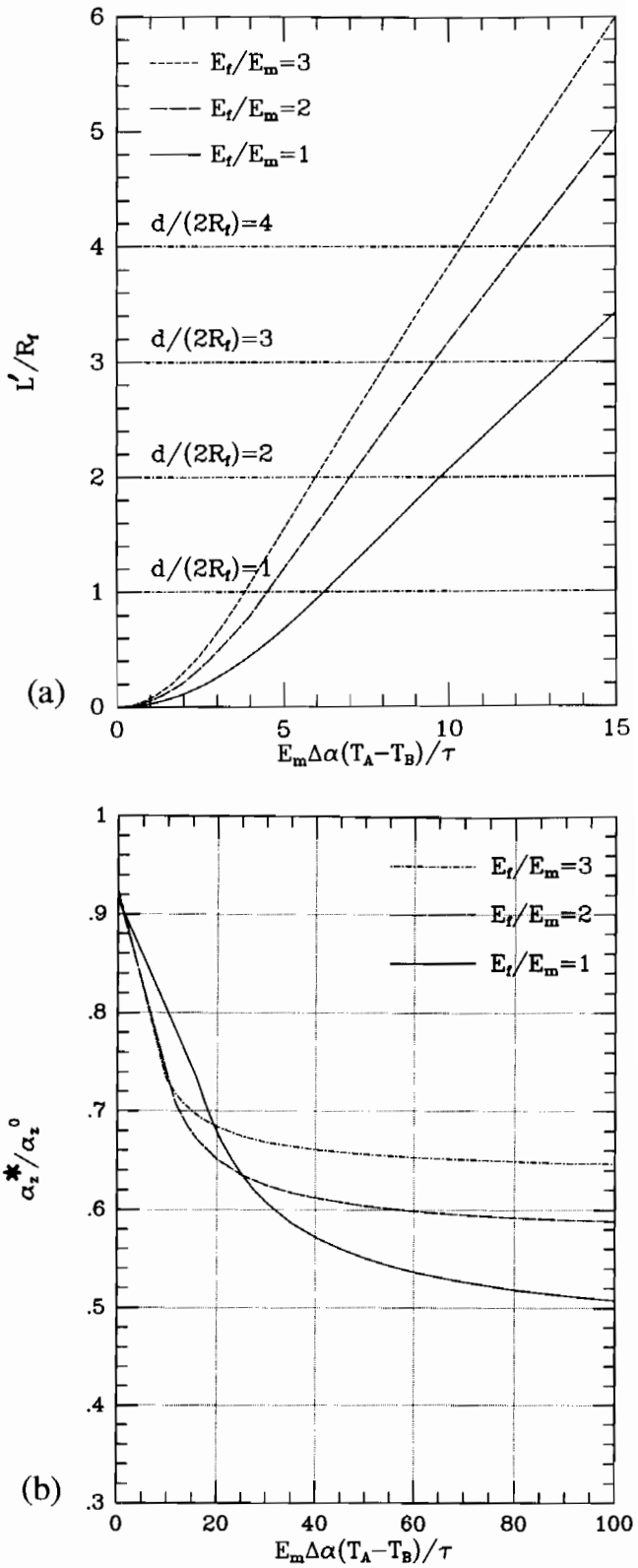

Figure 9 (a) Sliding zone length L' as a function of $E_m\Delta\alpha(T_A - T_B)/\tau$ for three values of E_f/E_m. The constitutive parameters used are $\lambda = \eta = 1$, $\rho = 0.3$ and $\nu_f = \nu_m = 0.3$. (b) Effective axial CTE of a cracked unidirectional composite under cyclic thermal loading as a function of $E_m\Delta\alpha(T_A - T_B)/\tau$ for three values of E_f/E_m. The constitutive parameters used are $\lambda = \eta = 1$, $\rho = 0.3$, $d/R_f = 8$ and $\nu_f = \nu_m = 0.3$

$$\frac{E_m \Delta\alpha (T_A - T_B)}{\tau} = \frac{2}{H}\frac{d}{R_f} \tag{31}$$

Thus, if $E_m\Delta\alpha(T_A - T_B)/\tau$ is significantly less than $2d/(HR_f)$, sliding will be negligible, while if this parameter is comparable to or greater than $2d/(HR_f)$, sliding will be important.

SUMMARY REMARKS

The work here has been directed at the combined effects of matrix cracking and fibre sliding on the thermal expansion behaviour of unidirectionally reinforced fibre/matrix composites. The focus is on systems where the CTE of the fibre is smaller than that of the matrix, such that matrix cracking and fibre sliding reduce the axial CTE of the composite and sliding will be resisted by friction. Combinations of cracking and sliding can reduce the axial CTE of the composite to a value close to that of the fibre. The radial component of the CTE is relatively unaffected.

When matrix cracking is unaccompanied by sliding, a fairly high density of cracks must be present to cause a significant reduction in the axial CTE of the composite. Typically, the matrix cracks must have a spacing d as small as about three times the fibre radius if the axial CTE is to be reduced half way to the fibre CTE. This is a relatively high crack density which is only rarely observed. A related observation emerging from the present work is that matrix crack interaction is not strong as long as $d > 3R_f$, and, consequently, the simpler analytical approximations based on the assumption of dilute matrix cracking are usually adequate. Sliding accompanying matrix cracking contributes significantly to the reduction in the axial CTE of the composite. If the debond toughness of the interface is relatively low, or if debonding has occurred earlier in the composite's loading history, the essential parameter for assessing the extent to which sliding reduces the axial CTE is $E_m\Delta\alpha\Delta T/\tau$. In particular, for repetitive thermal cycling between T_A and T_B, the conditions listed in connection with equation (31) can be used to gauge where the effective axial CTE lies between those of the undamaged composite and the fibre.

Similar considerations should apply to fibre-reinforced laminates such as cross-plies. Matrix cracking accompanied by fibre sliding will bring about a reduction in the CTE in the direction, or directions, perpendicular to the cracks. The parameter $E_m\Delta\alpha\Delta T/\tau$ will continue to be relevant.

A number of overly simplistic assumptions have been made in developing the model. The model does not account for effects of non-uniform matrix crack spacing or for non-uniform fibre distribution. Perhaps the most serious shortcoming is the assumption that the friction stress is independent of temperature. Temperature changes will result in changes in the normal stress acting across the fibre–matrix interface and are therefore expected to have some effect on the friction stress.

ACKNOWLEDGEMENTS

This work was supported in part by ARPA URI (subagreement P.O. #KK 3007) with the University of California, Santa Barbara, ONR Prime Contract N00014-92-J-1808, and by the Division of Applied Sciences, Harvard University. The ABAQUS finite element code was used in carrying out some of the cell model computations.

REFERENCES

1 Herakovich, C.T. and Hyer, M.W. *Eng. Fract. Mech.* 1986, **4**, 872
2 Hashin, Z. *Compos. Sci. Technol.* 1988, **31**, 247
3 Hutchinson, J.W. and Jensen, H.M. *Mech. Mater.* 1990, **9**, 139
4 He, M.Y., Wu, B.-X., Evans, A.G. and Hutchinson, J.W. *Mech. Mater.* 1994, **18**, 213
5 Pagano, N.J. and Brown, H.W. III *Composites* 1993, **24**, 69
6 Bowles, D.E. and Tompkins, S.S. *J. Compos. Mater.* 1989, **23**, 370
7 Rosen, B.W. and Hashin, Z. *Int. J. Eng. Sci.* 1970, **8**, 157
8 Laws, N. and Dvorak, G.J. *J. Compos. Mater.* 1988, **22**, 900
9 McMeeking, R.M. and Evans, A.G. *Mech. Mater.* 1990, **9**, 217
10 McCartney, L.N. *J. Mech. Phys. Solids* 1992, **40**, 27

NOTATION

a_i, b_i, c_i	dimensionless coefficients – see ref. 9
d	matrix crack spacing
D_i, D_i'	dimensionless coefficients
E_f, E_r	axial and radial moduli of fibre
E_m	modulus of matrix
K_{II}	mode II stress intensity factor
l	debond length
L, L', L''	length of current sliding zone
R_f, R	radii of fibre and cylindrical cell
T_0, T	'bonding' and current temperatures
α_z^f, α_r^f	axial and radial CTEs of fibre
α_m	CTE of matrix
α_z, α_r	axial and radial effective CTEs of cracked composite
α_z^0, α_r^0	axial and radial effective CTEs of uncracked composite
$\Delta\alpha = \alpha_z^f - \alpha_m$	thermal expansion mismatch
$\zeta_f = (1 - \nu_r)\eta$	parameter for transversely isotropic fibre
$\eta \equiv E_f/E_r$	modulus ratio for transversely isotropic fibre
$\lambda \equiv \alpha_r^f/\alpha_z^f$	CTE ratio for transversely isotropic fibre
ν_f, ν_r, ζ_f	Poisson ratios of transversely isotropic fibre – see equations (1) and (5)
ν_m	Poisson's ratio of matrix
ξ	dimensionless coefficient – see equation (7b)
$\rho = (R_f/R)^2$	fibre volume fraction
τ	fibre–matrix sliding shear resistance

APPENDIX: SHEAR-LAG ANALYSIS FOR PERFECTLY BONDED FIBRE–MATRIX INTERFACES

The shear-lag model has been widely applied to study the fracturing behaviour of fibre-reinforced composites. Here it is modified to solve for the stress field in the fibre caused by a uniform temperature change ΔT in a unidirectional composite as a function of matrix crack spacing, d. A formulation for the case of perfect fibre–matrix bonding is presented. This is extended in the body of the paper to cover interfacial debonding with frictional sliding. Several approximations are made in the course of the derivation to simplify the problem. The

accuracy of the end results are assessed with the aid of selected finite element calculations in *Figure 5*. Our approach is similar in a number of aspects to those of Laws and Dvorak[8] and McCartney[10] for transverse cracking in cross-ply laminates.

Let $\sigma_f(r,z)$ be the axial stress in the fibre, and let $\bar{\sigma}_f(z)$ be its average over the cross-section. With $\tau_i(z)$ as the shear stress on the fibre–matrix interface, equilibrium requires

$$\frac{d\bar{\sigma}_f}{dz} = -\frac{2\tau_i(z)}{R_f} \tag{A1}$$

We can approximate the shear stress distribution within the fibre as

$$\tau(r,z) = \frac{r\tau_i(z)}{R_f} \tag{A2}$$

We will neglect the influence of radial displacement of the fibre on the composite response by taking u_r to be zero. With $w(r,z) \equiv u_z$ as the axial displacement in the fibre, the shear strain in the fibre is $\gamma = \partial w/\partial r$. Thus, from equation (A2)

$$\tau(r,z) = \frac{r\tau_i(z)}{R_f} = G_f\frac{\partial w}{\partial r} \tag{A3}$$

which implies that

$$w(r,z) = w(0,z) + \frac{r^2\tau_i(z)}{2G_fR_f} \tag{A4}$$

Then, because $\sigma_f = E_f\partial w/\partial z$, it follows that

$$\sigma_f(r,z) = \sigma_{f0}(z) + \frac{r^2}{R_f^2}[\sigma_{fi}(z) - \sigma_{f0}(z)] \tag{A5}$$

where σ_{f0} and σ_{fi} are, respectively, the axial stress in the fibre at the centre and at the interface. Note that the average stress is given by

$$\bar{\sigma}_f = \frac{1}{2}(\sigma_{f0} + \sigma_{fi}) \tag{A6}$$

Next, we use equations (A1)–(A3) and (A5) to obtain

$$\frac{d^2\bar{\sigma}_f}{dz^2} = -\frac{1}{R_f(1+\nu_f)}\left[\frac{\partial\sigma_f}{\partial r}\right]_{r=R_f} = -\frac{2}{R_f^2(1+\nu_f)}(\sigma_{fi} - \sigma_{f0}) \tag{A7}$$

Assuming that the matrix stress σ_m is independent of radial distance r, continuity of axial strain at the fibre–matrix interface, $r = R_f$, requires

$$\frac{\sigma_{fi}}{E_f} = \frac{\sigma_m}{E_m} \tag{A8}$$

Equations (A6) and (A8), together with the overall equilibrium condition

$$(1-\rho)\sigma_m + \rho\bar{\sigma}_f = 0 \tag{A9}$$

enable one to solve σ_{fi} and σ_{f0} in terms of average fibre stress $\bar{\sigma}_f$. With this result in hand, the governing differential equation (A7) finally becomes

$$\frac{d^2\bar{\sigma}_f}{dz^2} = \frac{4E}{E_mR_f^2(1-\rho)(1+\nu_f)}\bar{\sigma}_f \tag{A10}$$

Equation (A10) is now solved with the boundary condition

$$\bar{\sigma}_f = a_2E_m\Delta\alpha\Delta T \quad \text{at} \quad z = \pm d/2 \tag{A11}$$

to get

$$\bar{\sigma}_f(z) = a_2E_m\Delta\alpha\Delta T\frac{\cosh(kz)}{\cosh(kd/2)} \tag{A12}$$

where

$$k = \left(\frac{4E}{E_mR_f^2(1-\rho)(1+\nu_f)}\right)^{1/2} \tag{A13}$$

and the non-dimensional coefficient a_2 is defined in HJ. The additional strain due to matrix cracking in the cell element is given by

$$\Delta = \frac{2}{d}\int_0^{d/2}\frac{\bar{\sigma}_f}{E_f}dz = \frac{E_m\Delta\alpha\Delta T(1-\rho)}{E}\frac{\tanh(kd/2)}{kd/2} \tag{A14}$$

From (A14), the effective longitudinal thermal expansion coefficient of the cracked composite is readily obtained as

$$\alpha_z = \alpha_z^0 + \frac{E_m(1-\rho)(\alpha_f - \alpha_m)}{E}\frac{\tanh(kd/2)}{kd/2} \tag{A15}$$

which approaches α_f as $d \to 0$.

So far the transverse displacement of the fibre due to temperature change has been taken to be zero. As a first approximation, however, one can substitute the fibre stress (A12) into the relation $\sigma_r = b_1\sigma_f$ given by HJ and calculate the resulting average strain in the radial direction. An approximate solution for the effective CTE in the transverse direction is thus obtained as

$$\alpha_r = \alpha_r^0 + \xi\frac{E_f(1-\rho)(\alpha_f - \alpha_m)}{E}\frac{\tanh(kd/2)}{kd/2} \tag{A16}$$

where the dimensionless coefficient ξ has been defined in equation (7b).